



CHORUS

This is the accepted manuscript made available via CHORUS. The article has been published as:

Geometrically induced transitions between semimetal and semiconductor in graphene

Marc Dvorak and Zhigang Wu

Phys. Rev. B **90**, 115415 — Published 12 September 2014

DOI: [10.1103/PhysRevB.90.115415](https://doi.org/10.1103/PhysRevB.90.115415)

Transitions between Semimetal and Semiconductor in Graphene Induced Geometrically

Marc Dvorak and Zhigang Wu*

Department of Physics, Colorado School of Mines, Golden, CO 80401, USA

(Dated: August 27, 2014)

Abstract

How the long-range ordering and local defect configurations modify the electronic structure of graphene remains an outstanding problem in nanoscience, which precludes the practical method of patterning graphene from being widely adopted for making graphene-based electronic and optoelectronic devices, because a small variation in supercell geometry could change the patterned graphene from a semimetal to a semiconductor, or vice versa. Based on the effective-Hamiltonian formalism, here we reveal that a semimetal-to-semiconductor transition can be induced geometrically without breaking the sublattice symmetry. For the same patterning periodicity, however, breaking the sublattice symmetry increases the gap, while phase cancellation can lead to a semiconductor-to-semimetal transition in non-Bravais lattices. Our theory predicts the analytic relationship between the long-range defects ordering and bandgap opening/closure in graphene, which is in excellent agreement with our numerical *ab initio* calculations of graphene nanomeshes and partially hydrogen passivated or boron nitride doped graphene.

PACS numbers: 73.22.Pr, 73.22.-f, 71.15.Mb

I. INTRODUCTION

While graphene^{1,2} possesses exceptional charge carrier mobilities³, it lacks a sizable bandgap necessary for meaningful on-off ratios in field-effect transistors or for practical optoelectronics. The pursuit of semiconducting graphene-based materials remains a high priority in current research. Recently, field-effect transistors based on graphene nanomeshes (GNMs), in which periodic holes are punctuated, have been fabricated⁴. Similarly, bandgap opening in graphene has also been induced by patterned hydrogen (H) adsorption⁵ or boron nitride (BN) doping⁶⁻⁸. An alternative scheme is ‘self-doping’, where extended defects, such as pentagons and heptagons, are introduced to alter the properties of graphene⁹.

An outstanding problem is how such periodic patternings modify the electronic structure of graphene, in particular, what are the exact effects of the long-range ordering and local defects on the Dirac points (\mathbf{K} and \mathbf{K}') where π and π^* bands touch? Previous experimental^{4,5,8,10,11} and theoretical¹²⁻²⁶ studies have revealed that the electronic band structure of graphene is sensitive to patterning: a small variation in the supercell periodicity could change the patterned graphene from a semimetal to a semiconductor, or vice versa. However, the underlying mechanisms and basic rules remain unclear, since most of these theoretical efforts are largely computation-driven and empirical, relying heavily on first-principles computations of special cases and thus lacking analytic understanding from fundamental considerations.

Here we propose a theory based on the effective Hamiltonian for the tight-binding model of graphene to reveal the analytic relation between defect geometry and bandgap opening/closure. We show that without breaking the sublattice symmetry, the semimetal-to-semiconductor transition can occur if the periodic defects induce scattering between two sublattices at the Dirac points, while such scattering could be annihilated by phase cancellation if defects form non-Bravais lattices in certain arrangements. In addition, breaking the sublattice symmetry always increases bandgaps, and such symmetry breaking and restoring can also be induced geometrically. We then carry out first-principles electronic structure calculations for three different types of patterned graphene including GNMs and partially H-passivated and BN-doped graphene. The numerical results confirm our analytic theory and find the bandgap scaling rules in these defected graphene structures as well.

II. THEORETICAL RESULTS

Two carbon (C) atoms in the unit cell of graphene form two sublattices, and the famous electronic band structure of graphene is well described by the two-dimensional tight-binding model Hamiltonian^{2,27} including only the nearest-neighbor hopping:

$$H_0(\mathbf{k}) = \begin{pmatrix} E_0 & \lambda f(\mathbf{k}) \\ \lambda f^*(\mathbf{k}) & E_0 \end{pmatrix}. \quad (1)$$

Here E_0 and λ are the onsite energy and hopping parameter, respectively, and

$$f(\mathbf{k}) = e^{ik_x a} + 2e^{-ik_x a/2} \cos\left(\frac{\sqrt{3}}{2}k_y a\right), \quad (2)$$

with a the C-C distance. The eigenvalues for this effective Hamiltonian are $E = E_0 + s\lambda|f(\mathbf{k})|$, where $s = \pm 1$, and the eigenstates are

$$\langle \mathbf{r} | s, \mathbf{k} \rangle = \frac{1}{\sqrt{2}} e^{i\mathbf{k} \cdot \mathbf{r}} \begin{pmatrix} 1 \\ s e^{i\theta(\mathbf{k})} \end{pmatrix}, \quad (3)$$

where $e^{i\theta(\mathbf{k})} = f(\mathbf{k})/|f(\mathbf{k})|$.

All types of periodic patterning mentioned above can be universally modeled by applying a periodic external potential $U(\mathbf{r}) = U(\mathbf{r} + \mathbf{R}_i)$, with \mathbf{R}_i ($i = 1, 2$) the supercell lattice vectors for the patterned graphene. The scattering amplitude between two states is²⁸⁻³¹

$$\langle s, \mathbf{k} | U(\mathbf{r}) | s', \mathbf{k}' \rangle = \sum_{\mathbf{G}} \frac{1}{2} (1 + s s' e^{i[\theta(\mathbf{k}') - \theta(\mathbf{k})]}) U(\mathbf{G}) \delta_{\mathbf{k}', \mathbf{k} - \mathbf{G}}, \quad (4)$$

where \mathbf{G} and $U(\mathbf{G})$ are the reciprocal lattice vector and the Fourier component of the external periodic potential, respectively.

Eq. 4 suggests that a semimetal to semiconductor transition can occur if the scattering between two degenerate states at Dirac points \mathbf{K} and \mathbf{K}' is non-zero, i.e., when $U(\mathbf{G}) \neq 0$ at $\mathbf{G} = \mathbf{K} - \mathbf{K}'$. Because of the periodicity in the reciprocal space of the pristine graphene, the above condition is equivalent to $U(\mathbf{K}) \neq 0$ [and $U(\mathbf{K}') \neq 0$], which induces bandgap opening without breaking the sublattice symmetry. Considering the usual case in which the defected sites are only a small portion of all C atoms, we propose a simple periodic model potential based on the Dirac δ -function,

$$U(\mathbf{r}) = \sum_{\alpha, \beta = -\infty}^{\alpha, \beta = +\infty} g \delta(\mathbf{r} - \alpha \mathbf{R}_1 - \beta \mathbf{R}_2), \quad (5)$$

with integers α and β . $U(\mathbf{K}) \neq 0$ only when the reciprocal lattice vectors \mathbf{G} for the periodically modified graphene, with lattice vectors $\mathbf{R}_1 = n_1\mathbf{a}_1 + m_1\mathbf{a}_2$ and $\mathbf{R}_2 = n_2\mathbf{a}_1 + m_2\mathbf{a}_2$, contain Dirac points of the pristine graphene. Here \mathbf{a}_1 and \mathbf{a}_2 are primitive lattice vectors of the pristine graphene, and n_1, m_1, n_2 and m_2 are 4 integers. It is straightforward to show³² that $U(\mathbf{K}) \neq 0$ is satisfied only when

$$n_1 - m_1 = 3p, \text{ and } n_2 - m_2 = 3q, \quad (6)$$

for integers p and q , which is the same condition for a *semimetallic* carbon nanotube with chirality index (n_1, m_1) or (n_2, m_2) at the tight-binding level of theory.

Therefore there are two approaches to open up a bandgap in graphene by applying periodic defects. The first one is sublattice symmetry breaking, e.g., BN doping, so that the two diagonal matrix elements in the effective Hamiltonian (Eq. 1) are different and the degeneracy at the Dirac points is lifted. This has been extensively studied. The second is the inter-valley scattering between two Dirac points \mathbf{K} and \mathbf{K}' induced geometrically without breaking the sublattice symmetry, which can be realized in GNMs and partially H-doping. The second mechanism remains under exploration, and previous works^{28–31} concluded that this mechanism could *not* open up a bandgap since smooth external potentials were used to describe periodic defects, which is not true in general. Here we employed the δ -function potential and derived the analytical relations between the long-range ordering and the transition between semimetal and semiconductor.

Next we extend our theory for graphene sheets whose defects form non-Bravais lattices, e.g., a honeycomb structure. There are more than one ($M > 1$) defects in a supercell, which are centered at $\boldsymbol{\tau}_1, \boldsymbol{\tau}_2, \dots, \boldsymbol{\tau}_M$, and it can be shown that

$$U^{\text{non-Brav}}(\mathbf{k}) = S(\mathbf{k})U^{\text{Brav}}(\mathbf{k}), \quad (7)$$

where $U^{\text{non-Brav}}(\mathbf{k})$ is the external potential for a non-Bravais lattice, $U^{\text{Brav}}(\mathbf{k})$ for the corresponding Bravais lattice, and the defect structure factor $S(\mathbf{k}) = \sum_{j=1}^M \exp(i\mathbf{k} \cdot \boldsymbol{\tau}_j)$. Thus even if the lattice vectors of a non-Bravais structure satisfy the bandgap opening condition (Eq. 6), a zero structure factor at the Dirac point,

$$0 = S(\mathbf{K}) = \sum_{j=1}^M \exp(i\mathbf{K} \cdot \boldsymbol{\tau}_j), \quad (8)$$

leads to bandgap closure due to phase cancellation.

III. AB INITIO SIMULATION RESULTS

We employ first-principles electronic structure calculations based on the density functional theory (DFT) to verify our analytic theory. Although DFT often severely underestimate bandgaps, it accurately predicts a zero gap at the Dirac points for graphene and yields qualitatively correct electronic band structures for graphene³³ and graphene nanoribbons^{34,35}. The spin-polarized calculations within the generalized gradient approximation³⁶ are carried out using the SIESTA code³⁷ based on atomic orbitals. Specifically, we use a triple- ζ polarized basis set for C and double- ζ polarized basis sets for B, N, and H, whose accuracy and convergence have been well examined by comparing against calculations using the planewave VASP code³⁸. All graphene structures in this work are relaxed until all atomic forces are less than 0.02 eV/Å and the maximum stress is below 0.2 GPa.

A. Defects Forming Bravais Structures

Fig. 1 shows the crystal and electronic band structures for two different supercells with partial H-passivation, holes (GNMs), and BN doping regions forming Bravais lattices. The effect of supercell lattice symmetry on electronic properties is compared across the three rows of panels, while the effect of different types of defects is compared among each column. The supercells on the left column have $(n_1, m_1, n_2, m_2) = (6, -6, 4, 4)$ so that $n_1 - m_1$ and $n_2 - m_2$ are both divisible by 3, satisfying the condition of Eq. 6, while the supercells on the right column have $(n_1, m_1, n_2, m_2) = (7, -7, 4, 4)$, therefore $n_1 - m_1 = 14$, not divisible by 3. Our theory predicts that the partially H-passivated graphene and GNM shown in the left column of Fig. 1 are semiconductors, while those on the right (Figs. 1b and 1d) are semimetals, consistent with first-principles results. Our theory also indicates that the BN-doped graphene is always semiconducting, but the the long-range ordering could increase E_g if the lattice parameters (n_1, m_1, n_2, m_2) satisfy Eq. 6, agreeing well with calculated electronic band structures shown in Figs. 1e and 1f, with $E_g = 0.78$ and 0.39 eV, respectively.

In addition, as expected, electronic band structures in the left three panels are very similar, different mainly in values of bandgap, with 0.55, 0.56 and 0.78 eV for the partially-H passivated graphene, GNM, and BN-doped graphene shown in Figs. 1a, 1c and 1e, respectively. Electronic band structures across the right column are also very similar, except

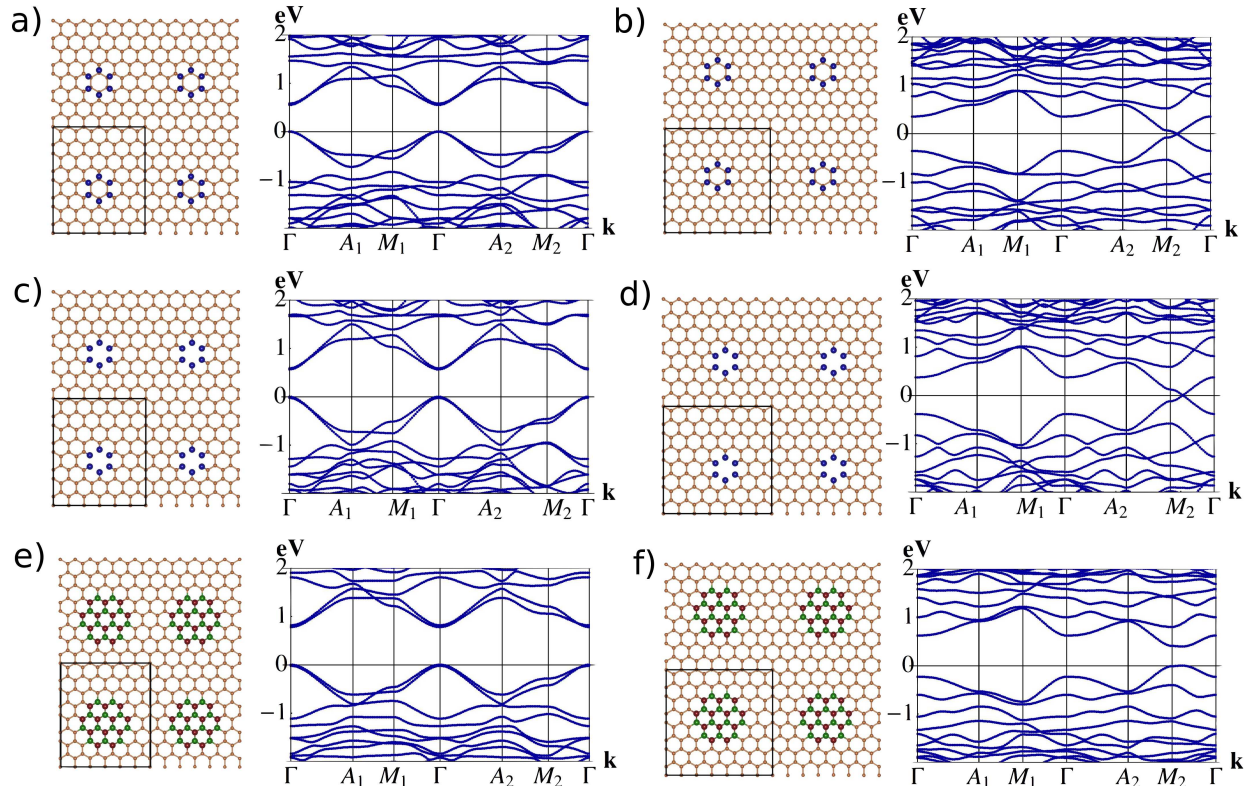


FIG. 1. (color online) Crystal (left) and electronic band (right) structures for (a) H-passivated graphene, (c) GNM and (e) BN-doped graphene with supercell lattice parameters $(n_1, m_1, n_2, m_2) = (6, -6, 4, 4)$. Panels (b), (d) and (f) show those corresponding structures with $(n_1, m_1, n_2, m_2) = (7, -7, 4, 4)$. Here C, H, B and N atoms are denoted by golden, blue, green and red spheres, respectively. The black rectangle in each panel indicates the supercell of defected graphene.

that in Fig. 1f for the BN-doped graphene there is an energy gap at a point between Γ and M_2 , at which bandgap closes in Figs. 1b and 1d for H-passivated graphene and GNM. These three types of defected graphene structures with other shapes of supercells, such as hexagonal and parallelogram, show the same trends for electronic band structures.

Tables I and II summarize the calculated E_g for H-passivated and BN-doped graphene sheets with various supercell symmetries, in addition to the rectangular unit cells shown in Fig. 1. Results for GNM structures (not shown) are very similar to those for H-passivated graphene, as demonstrated in Figs. 1a–d and in Fig. 2a. Here armchair indicates that both supercell vectors are along the armchair direction so that $(n_1, m_1, n_2, m_2) = (2n, -n, m, m)$

TABLE I. Calculated band gaps (E_g in eV) of graphene sheets partially passivated by H. Here N_d and N_{tot} are the numbers of defected (passivated by H) and total carbon atoms in one supercell, respectively.

Cell type	n_1	m_1	n_2	m_2	E_g	N_d	N_{tot}	Defect %
Armchair	10	-5	5	5	0.48	12	150	8.0
	14	-7	8	8	0.14	6	336	1.8
	8	-4	5	5	0.59	12	120	10.0
Zigzag	6	0	0	6	0.71	6	72	8.3
	6	0	0	6	1.05	12	72	16.7
	6	0	0	7	0.00	12	84	14.3
	7	0	0	7	0.00	12	98	12.2
Chiral hexagonal	3	5	8	3	0.00	6	62	9.7
	5	4	9	-5	0.00	6	122	4.9
	7	1	8	-7	0.49	6	114	5.3
Chiral rectangular	6	2	-7	5	0.00	12	88	13.6
	6	3	-4	5	0.63	6	84	7.1
	6	4	-7	8	0.00	6	152	3.9
Rectangular	5	-5	5	5	0.00	6	100	6.0
	6	-6	4	4	0.55	6	96	6.3
	7	-7	4	4	0.00	6	112	5.4
Parallelogram	6	1	-3	9	0.00	6	114	5.3
	6	2	-3	9	0.00	6	120	5.0
	6	3	-2	7	0.54	6	96	6.3

with n and m two integers, while zigzag indicates that both supercell vectors are along the zigzag direction so that $(n_1, m_1, n_2, m_2) = (n, 0, 0, m)$. Rectangular corresponds to rectangular supercells with one lattice vector along the zigzag direction while the other vector is along the armchair direction with $(n_1, m_1, n_2, m_2) = (n, -n, m, m)$, while chiral rectangular and chiral hexagonal correspond to rectangular and hexagonal supercells with

TABLE II. Calculated band gaps (E_g in eV) of graphene sheets doped by BN. Here N_d is the number of defected (replaced by B or N) carbon atoms while N_{tot} indicates the total number of atoms (including C, B and N) in one supercell.

Cell type	n_1	m_1	n_2	m_2	E_g	N_d	N_{tot}	Defect %
Armchair	10	-5	5	5	0.34	12	150	8.0
	14	-7	8	8	0.08	6	336	1.8
	8	-4	5	5	0.42	12	120	10.0
Zigzag	6	0	0	6	0.69	12	72	16.7
	6	0	0	7	0.41	12	84	14.3
	7	0	0	7	0.36	12	98	12.2
Chiral hexagonal	3	5	8	-3	0.16	6	98	6.1
	3	5	8	-3	0.48	12	98	12.2
	5	4	9	-5	0.13	6	122	4.9
	5	4	9	-5	0.38	12	122	9.8
	7	1	8	-7	0.25	6	114	5.3
	7	1	8	-7	0.68	12	114	10.5
Chiral rectangular	6	2	-7	5	0.42	12	104	11.5
	6	3	-4	5	0.33	6	84	7.1
	6	4	-7	8	0.31	12	152	7.9
Rectangular	5	-5	5	5	0.53	12	100	12.0
	6	-6	4	4	0.78	12	96	12.5
	7	-7	4	4	0.39	12	112	10.7
Parallelogram	6	1	-3	9	0.42	12	114	10.5
	6	2	-3	9	0.39	12	120	10.0
	6	3	-2	7	0.75	12	96	12.5

lattice vectors along arbitrary directions. These numerical results in Tables I and II have qualitatively verified our analytical modeling on the semimetal-to-semiconductor transition in periodically defected graphene.

Quantitatively, E_g in these semiconducting graphene structures are roughly proportional to the defect percentage (x , when $x \lesssim 15\%$): $E_g \approx Cx$ with C a constant, as demonstrated in Fig. 2. Here Fig. 2a shows that E_g in a semiconducting GNM is slightly larger than that in a corresponding H-passivated graphene with the same supercell and defected areas. Fig. 2a also emphasizes the sensitive dependence of E_g on lattice parameters which can dramatically switch these defected graphene between semiconductor and semimetal by small changes. However, Fig. 2b indicates that in a BN-doped graphene, for the same level of doping, E_g is considerably enhanced if its lattice parameters (n_1, m_1, n_2, m_2) satisfy Eq. 6. Linear fitting to Fig. 2a obtains $C = 0.091$ eV/% and 0.087 eV/% for GNM and H-passivated graphene, respectively, and $C = 0.057$ eV/% (the red line) and 0.036 eV/% (the green line) in Fig. 2b for BN-doped graphene. These values suggest that in the BN-doped graphene the imbalance between two sublattices contributes more to E_g than the supercell symmetry does, and the effect on E_g from the latter is much weaker than that in GNMs or H-passivated graphene, because apparently removing p_z orbitals or passivating p_z orbitals of C atoms causes much more dramatic changes on the graphene lattice than B/N substitution. We note that in semiconducting GNMs and H-passivated graphene E_g have much better linear relations to defect percentage than those for BN-doped graphene. This might also due to less severe perturbation induced by BN-doping than H-passivation or vacancy, complicating E_g as a function of BN doping percentage.

B. Defects Forming Non-Bravais Structures

Next we consider defects forming non-Bravais structures. As illustrated in Fig. 3, the H-passivated graphene sheets in the upper two panels share the same chiral hexagonal lattice with parameters $(n_1, m_1, n_2, m_2) = (7, 1, 8, -7)$. Their electronic band structures are similar, except that E_g for the non-Bravais structure is larger. Since $n_1 - m_1$ and $n_2 - m_2$ are both divisible by 3, the Bravais structure (Fig. 3a) is semiconducting with $E_g = 0.50$ eV, while the non-Bravais structure (Fig. 3b) with two passivated areas has a larger gap of 0.84 eV. This is because $\boldsymbol{\tau}_2 - \boldsymbol{\tau}_1 = 2\mathbf{a}_1 + 2\mathbf{a}_2$, and $S(\mathbf{K}) = e^{i\mathbf{K}\cdot\boldsymbol{\tau}_1}[1 + e^{i\mathbf{K}\cdot(\boldsymbol{\tau}_2 - \boldsymbol{\tau}_1)}] = e^{i\mathbf{K}\cdot\boldsymbol{\tau}_1}(1 + e^{i4\pi})$, leading to $|S(\mathbf{K})| = 2 > 1$; consequently, constructive interference enlarges the bandgap.

One cannot create a non-Bravais graphene lattice with two identical defects per unit cell whose structure factor vanishes at the Dirac point. This is because for an arbitrary

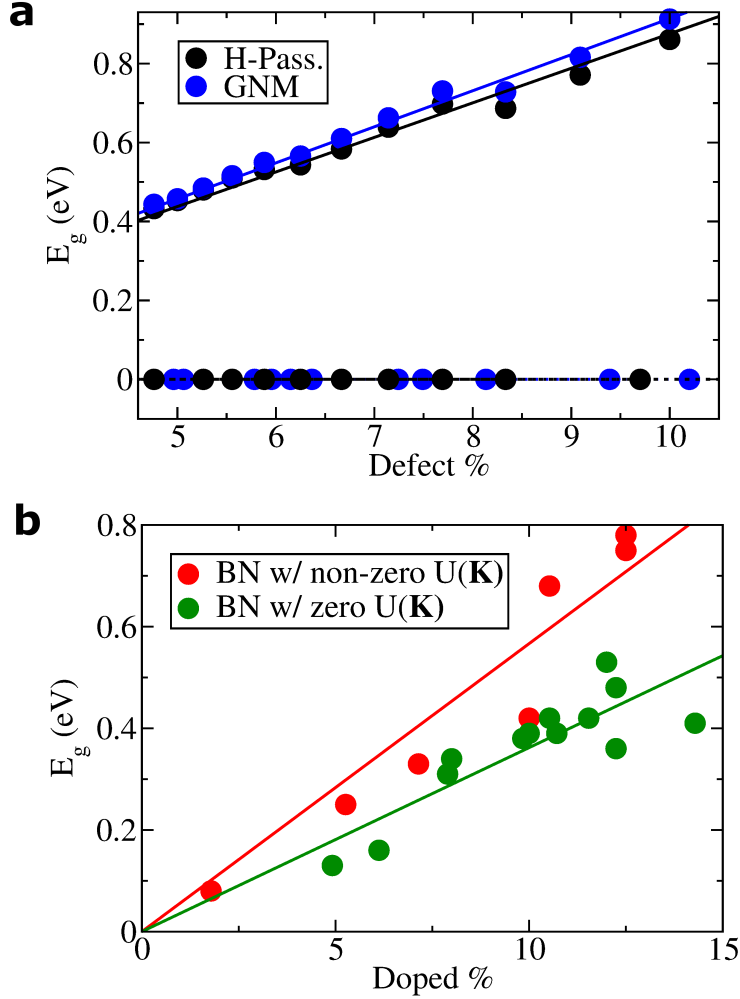


FIG. 2. (color online) Bandgap (E_g) as a function of defect percentage for (a) partially H-passivated graphene and GNMs and (b) BN-doped graphene.

relative displacement $\boldsymbol{\tau}_2 - \boldsymbol{\tau}_1 = p\mathbf{a}_1 + q\mathbf{a}_2$ with p and q two integers, $\mathbf{K} \cdot (\boldsymbol{\tau}_2 - \boldsymbol{\tau}_1) = 2q\pi + \frac{4}{3}(p - q)\pi \neq (2n + 1)\pi$ with n an integer, thus $S(\mathbf{K}) = 1 + e^{i\mathbf{K} \cdot (\boldsymbol{\tau}_2 - \boldsymbol{\tau}_1)} \neq 0$. However, it is possible when there are more than two identical defects per unit cell, e.g., the triangular arrangement shown in Fig. 3d. In this H-passivated graphene, defects are displaced along zigzag directions in a supercell by vectors of $\boldsymbol{\tau}_2 - \boldsymbol{\tau}_1 = 5\mathbf{a}_1$ and $\boldsymbol{\tau}_3 - \boldsymbol{\tau}_1 = 5\mathbf{a}_2$, so that $1 + e^{i\mathbf{K} \cdot (\boldsymbol{\tau}_2 - \boldsymbol{\tau}_1)} + e^{i\mathbf{K} \cdot (\boldsymbol{\tau}_3 - \boldsymbol{\tau}_1)} = 0$. Even though the corresponding Bravais structure (not shown) is semiconducting with $E_g = 0.34$ eV, this non-Bravais structure is a semimetal. In contrast, the non-Bravais structure plotted in Fig. 3c, in which three defects in a supercell are displaced along armchair directions, specifically, $\boldsymbol{\tau}_2 - \boldsymbol{\tau}_1 = 2\mathbf{a}_1 + 2\mathbf{a}_2$ and $\boldsymbol{\tau}_3 - \boldsymbol{\tau}_1 = 2\mathbf{a}_1 - 2\mathbf{a}_2$,

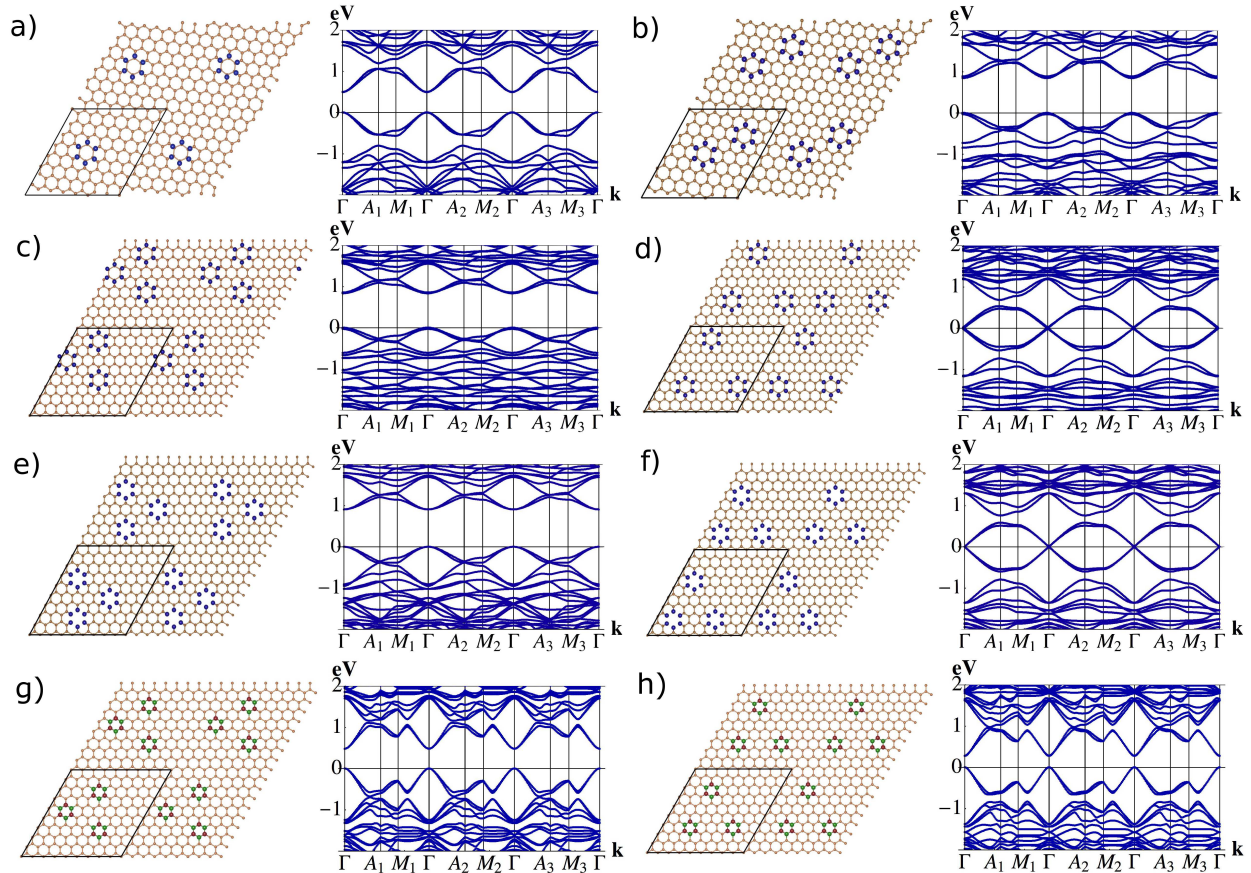


FIG. 3. (color online) Crystal (left) and electronic band (right) structures of defected graphene sheets, which have $(7, 1, 8, -7)$ supercells in (a) and (b) and $(9, 0, 0, 9)$ supercells in (c–h). Except for panel (a), defects in these graphene structures form non-Bravais lattices. (a–d) H-passivated graphene. (e) and (f) GNMs. (g) and (h) BN-doped graphene. Supercells in these graphene structures are indicated by black rhombuses.

leading to $|S(\mathbf{K})| = \sqrt{3}$ and an enlarged bandgap of 0.83 eV.

Fig. 3e suggests that a constructive interference with $|S(\mathbf{K})| = \sqrt{3}$ in the GNM leads to an enhanced $E_g = 0.91$ eV, compared with $E_g = 0.36$ eV for the corresponding Bravais GNM, whereas a destructive interference with $S(\mathbf{K}) = 0$ in the non-Bravais GNM plotted in Fig. 3f leads to a zero gap. Thus our calculations have demonstrated a transition from semiconductor to semimetal by rearranging the defects in H-passivated graphene and GNMs, as predicted in Eq. 8.

Finally we discuss non-Bravais lattices with BN-doped areas. Fig. 3g indicates a constructive interference with $|S(\mathbf{K})| = \sqrt{3}$ drastically increases bandgap ($E_g = 0.48$ eV),

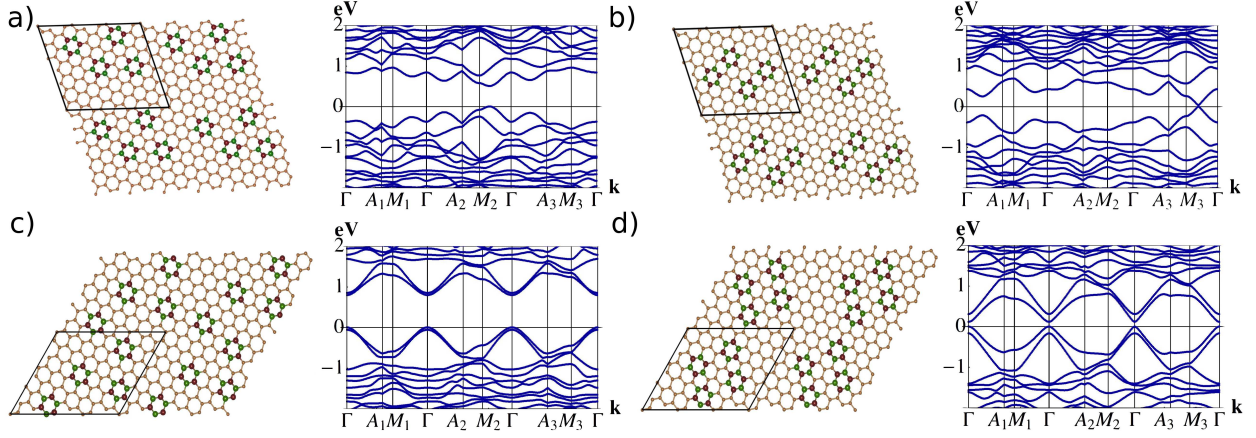


FIG. 4. (color online) Crystal (left) and electronic band (right) structures of BN-doped graphene with supercell lattice parameters of $(6, 1, -3, 9)$ in (a) and (b) and $(6, 3, -2, 7)$ in (c) and (d). In the left column [(a) and (c)] four doped areas in a supercell are identical, while in the right column [(b) and (d)] in a supercell two BN-doped areas are different from the other two so that an overall balance between A and B -sublattices are reached. In each panel the supercell is indicated by a black rhomboid.

compared with that of only 0.17 eV in the corresponding Bravais structure. However, a destructive interference with zero $S(\mathbf{K})$ doesn't lead to a zero gap at the Γ -point (Fig. 3h), although its bandgap is reduced to 0.27 eV. This is due to the imbalance between A - and B -sublattices, so that $E_g \neq 0$. Compared with the corresponding Bravais structure, the non-Bravais BN-doped graphene with $S(\mathbf{K}) = 0$ (Fig. 3g) has a larger gap, because of the increase in imbalance between A - and B -sublattices.

To induce a transition from semiconductor to semimetal for BN-doped graphene, one can geometrically restore the sublattice balance by switching B and N atoms between doped regions. Fig. 4b shows a $(6, 1, -3, 9)$ lattice with zero gap, compared with the structure plotted in Fig. 4a, which has the same $(6, 1, -3, 9)$ lattice but is a semiconductor with $E_g = 0.50$ eV. Figs. 4c and 4d show the $(6, 3, -2, 7)$ lattices, which satisfy the gap-opening rule of Eq.6. In Fig. 4a, $S(\mathbf{K}) \neq 0$, leading to a relatively large bandgap of 0.80 eV, whereas in Fig. 4d switching B and N atoms between defects to restore A - and B -sublattice balance significantly reduces E_g to merely 0.12 eV, and further arranging identical doping sites to ensure $S(\mathbf{K}) = 0$ can eventually induce the semiconductor-to-semimetal transition.

IV. SUMMARY

In summary, we find that the degeneracy at the Dirac points is lifted and a sizable bandgap appears when reciprocal lattice vectors of such a defected graphene overlap with Dirac points of the pristine graphene. Previous works have shown the absence of back scattering and bandgaps in graphene and metallic carbon nanotubes under external potentials that vary slowly on the order of the C-C bond length²⁸⁻³⁰. However, for dopants, adsorbed atoms and vacancies the corresponding effective potentials vary considerably on this length scale, leading to the existence of the inter-valley scattering between \mathbf{K}' appears.²⁸⁻³⁰ The symmetry breaking between two sublattices is also a contributing factor to bandgap, which has been studied before. Here our theory includes both sublattices asymmetry and inter-valley scattering. For multiple defects in a supercell forming the non-Bravais structure, the magnitude of the structure factor at the Dirac point determines the strength of long-range ordering induced non-degeneracy at the Dirac point, thus arranging defects positions in non-Bravais structures could cause a transition from semiconductor to semimetal if a destructive interference leads to a complete phase cancellation and the sublattice symmetry is kept.

Our *ab initio* electronic structure calculations on a variety of partially H-passivated graphene, graphene nanomeshes, and BN-doped graphene demonstrate the validity of our analytic analyses. Specifically, the sublattice symmetry in H-passivated graphene and GNMs we studied is maintained, therefore the supercell symmetry and the structure factor at the Dirac point can be controlled geometrically to induce transitions between semimetal and semiconductor. On the other hand, the balance between two sublattices in BN-doped graphene sheets must be restored to induce such transitions, in addition to lattice symmetry considerations. Present modeling not only offers the fundamental understanding of how the local defects configurations and long-range ordering modify the electronic properties of complex and realistic graphene structures so that precise tuning for various applications is possible, but also can be employed to investigate magnetism induced by patterning graphene.

ACKNOWLEDGMENTS

This work was supported by U.S. DOE Early Career Award (Grant No. DE-SC0006433). Computations were carried out at the Golden Energy Computing Organization at CSM and

the National Energy Research Scientific Computing Center (NERSC). The authors thank M. Lusk and D. Wood for insightful discussions.

* zhiwu@mines.edu

- ¹ A. K. Geim and K. S. Novoselov, *Nature Mater.* **6**, 183 (2007).
- ² A. H. Castro Neto, F. Guinea, N. M. R. Peres, K. S. Novoselov, and A. K. Geim, *Rev. Mod. Phys.* **81**, 109 (2009).
- ³ A. S. Mayorov, R. V. Gorbachev, S. V. Morozov, L. Britnell, R. Jalil, L. A. Ponomarenko, P. Blake, K. S. Novoselov, K. Watanabe, T. Taniguchi, and A. K. Geim, *Nano Lett.* **11**, 2396 (2011).
- ⁴ J. Bai, X. Zhong, S. Jiang, Y. Huang, and X. Duan, *Nat. Nanotech.* **5**, 190 (2010).
- ⁵ R. Balog, B. Jorgensen, L. Nilsson, M. Andersen, E. Rienks, M. Bianchi, M. Fanetti, E. Laegsgaard, A. Baraldi, S. Lizzit, Z. Sljivancanin, F. Besenbacher, B. Hammer, T. G. Pedersen, P. Hofmann, and L. Hornekaer, *Nature Mater.* **9**, 315 (2010).
- ⁶ X. Fan, Z. Shen, A. Q. Liu, and J.-L. Kuo, *Nanoscale* **4**, 2157 (2012).
- ⁷ R. Zhao, J. Wang, M. Yang, Z. Liu, and Z. Liu, *J. Phys. Chem. C* **116**, 21098 (2012).
- ⁸ L. Ci, L. Song, C. Jin, D. Jariwala, D. Wu, Y. Li, A. Srivastava, Z. F. Wang, K. Storr, L. Balicas, F. Liu, and P. M. Ajayan, *Nature Mater.* **9**, 430 (2010).
- ⁹ M. T. Lusk and L. D. Carr, *Phys. Rev. Lett.* **100**, 175503 (2008).
- ¹⁰ P. Sessi, J. R. Guest, M. Bode, and N. P. Guisinger, *Nano Lett.* **9**, 4343 (2009).
- ¹¹ H. Gao, L. Wang, J. Zhao, F. Ding, and J. Lu, *J. Phys. Chem. C* **115**, 3236 (2011).
- ¹² V. M. Pereira, J. M. B. Lopes dos Santos, and A. H. Castro Neto, *Phys. Rev. B* **77**, 115109 (2008).
- ¹³ V. M. Pereira, F. Guinea, J. M. B. Lopes dos Santos, N. M. R. Peres, and A. H. Castro Neto, *Phys. Rev. Lett.* **96**, 036801 (2006).
- ¹⁴ R. Martinazzo, S. Casolo, and G. F. Tantardini, *Phys. Rev. B* **81**, 245420 (2010).
- ¹⁵ M. Mirzadeh and M. Farjam, *J. Phys.: Condens. Matter* **24**, 235304 (2012).
- ¹⁶ M. Yang, A. Nurbawono, C. Zhang, Y. P. Feng, and Ariando, *App. Phys. Lett.* **96**, 193115 (2010).
- ¹⁷ J. M. Garcia-Lastra, *Phys. Rev. B* **82**, 235418 (2010).
- ¹⁸ J. Kang, J. Bang, B. Ryu, and K. J. Chang, *Phys. Rev. B* **77**, 115453 (2008).
- ¹⁹ J. A. Furst, J. G. Pedersen, C. Flindt, N. A. Mortensen, M. Brandbyge, T. G. Pedersen, and

- A.-P. Jauho, *New J. Phys.* **11**, 095020 (2009).
- ²⁰ R. Petersen, T. G. Pedersen, and A.-P. Jauho, *ACS Nano* **5**, 523 (2011).
- ²¹ F. Ouyang, S. Peng, Z. Liu, and Z. Liu, *ACS Nano* **5**, 4023 (2011).
- ²² R. Grassi, T. Low, and M. Lundstrom, *Nano Lett.* **11**, 4574 (2011).
- ²³ W. Oswald and Z. Wu, *Phys. Rev. B* **85**, 115431 (2012).
- ²⁴ B. Gharekhanlou, M. Alavi, and S. Khorasani, *Semicond. Sci. Tech.* **23**, 075026 (2008).
- ²⁵ B. Xu, Y. H. Lu, Y. P. Feng, and J. Y. Lin, *Journal of Applied Physics* **108**, 073711 (2010).
- ²⁶ S. Casolo, R. Martinazzo, and G. F. Tantardini, *The Journal of Physical Chemistry C* **115**, 3250 (2011), <http://pubs.acs.org/doi/pdf/10.1021/jp109741s>.
- ²⁷ P. R. Wallace, *Phys. Rev.* **71**, 622 (1947).
- ²⁸ T. Ando and T. Nakanishi, *Journal of the Physical Society of Japan* **67**, 1704 (1998).
- ²⁹ T. Ando, T. Nakanishi, and R. Saito, *Journal of the Physical Society of Japan* **67**, 2857 (1998).
- ³⁰ P. L. McEuen, M. Bockrath, D. H. Cobden, Y.-G. Yoon, and S. G. Louie, *Phys. Rev. Lett.* **83**, 5098 (1999).
- ³¹ C.-H. Park, L. Yang, Y.-W. Son, M. L. Cohen, and S. G. Louie, *Nature Phys.* **4**, 213 (2008).
- ³² M. Dvorak and Z. Wu, *Sci. Rep.* **3**, 2289 (2013).
- ³³ A. Grüneis, C. Attacalite, T. Pichler, V. Zabolotnyy, H. Shiozawa, S. L. Molodtsov, D. Inosov, A. Koitzsch, M. Knupfer, J. Schiessling, R. Follath, R. Weber, P. Rudolf, L. Wirtz, and A. Rubio, *Phys. Rev. Lett.* **100**, 037601 (2008).
- ³⁴ Y.-W. Son, M. L. Cohen, and S. G. Louie, *Phys. Rev. Lett.* **97**, 216803 (2006).
- ³⁵ L. Yang, C.-H. Park, Y.-W. Son, M. L. Cohen, and S. G. Louie, *Phys. Rev. Lett.* **99**, 186801 (2007).
- ³⁶ J. P. Perdew, K. Burke, and M. Ernzerhof, *Phys. Rev. Lett.* **77**, 3865 (1996).
- ³⁷ J. M. Soler, E. Artacho, J. D. Gale, A. Garcia, J. Junquera, P. Ordejón, and D. Sánchez-Portal, *J. Phys.: Condens. Matter* **14**, 2745 (2002).
- ³⁸ G. Kresse and J. Furthmüller, *Phys. Rev. B* **54**, 11169 (1996).